Supplementary Information

Broadening Through-Space Conjugation in Polyphosphates through α-Aminophosphonate Bridges for a Noteworthy Red Shift in Luminescence

Zheng Li, Pengfei Yang , Rui Wu, Qingyuan Meng, Jinyi Liu, Yan Zhao* and Hongxia Yan*

Xi'an Key Laboratory of Hybrid Luminescent Materials and Photonic Device, School of Chemistry and Chemical Engineering, Northwestern Polytechnical University, Xi'an 710129, Shaanxi, China. E-mail: hongxiayan@nwpu.edu.cn, zhaoyan@nwpu.edu.cn

Experimental Procedures

Materials and Testing Methods

The reagents involved in the experiment are listed in Table S1, and all purchased reagents were opened for the first time and used directly.

Table S1 Experimental materials and reagents

Reagent Name	Abbreviation	Specifications	Manufacturer
Dimethyl phosphonate	DMP	＞98%	Macklin Biochemical Co., Ltd
Diethylene glycol	DEG	＞98%	Macklin Biochemical Co., Ltd
Ethanol	EtOH	≥99.8%	Guanghua Sci-Tech Co., Ltd
Methanol	MeOH	99.99%	Guanghua Sci-Tech Co., Ltd
Ferric chloride hexahydrate	$FeCl_3{\cdot}_6H_2O$	99.9%	Tianli Chemical Reagents Ltd.
Copric chloride dihydrate	$CuCl_2{\cdot}2H_2O$	99.9%	Sinopharm Group Co. Ltd
Cobalt chloride hexahydrate	$CoCl_2{\cdot}_6H_2O$	99.9%	Sinopharm Group Co. Ltd
Barium chloride dihydrate	$BaCl_2{\cdot}2H_2O$	99.5%	Xi'an Chemical Reagent Factory Co. Ltd
Potassium chloride	KCl	99.8%	Tianli Chemical Reagents Ltd.
Aluminum chloride	$AlCl_3$	99 %	Tianli Chemical Reagents Ltd.
Sodium chloride	NaCl	99.9%	Tianli Chemical Reagents Ltd.
Mercury dichloride	$HgCl_2$	≥96%	Tianli Chemical Reagents Ltd.

Calcium chloride	$CaCl_2$	≥96%	Tianli Chemical Reagents Ltd.
Zinc chloride	$ZnCl_2$	99%	Tianli Chemical Reagents Ltd.
Chromium chloride hexahydrate	$CrCl_3 \cdot 6H_2O$	98%	Sinopharm Group Co. Ltd
n-Butylamine	NBA	≥99.5%	Macklin Biochemical Co., Ltd
p-Phenylenediamine	PPD	99%	Macklin Biochemical Co., Ltd
2-Hydroxy Benzaldehyde	Salicylaldehyde	99%	Macklin Biochemical Co., Ltd
distilled water	Water	--	Lab-prepared
Chloroform-d	$CDCl_3$	D,99.8 % +0.03% TMS	Macklin Biochemical Co., Ltd
Dimethyl sulfoxide-d_6	DMSO-d_6	D.99.7% +0.03% TMS	Macklin Biochemical Co., Ltd
N,N-Dimethylformamide	DMF	99.5 %	Macklin Biochemical Co., Ltd

In this study, the testing methods employed for polymer structure characterization and fluorescence property analysis are described below.

Determination of Molecular Weight and Its Distribution

The molecular weight and its distribution were determined using an Agilent 1260 Infinity II Gel Permeation Chromatography (GPC) system (USA). The principle relies on the size exclusion mechanism, where components in the sample have different retention times in the chromatographic column based on their relative molecular sizes. After separation, the polymer fractions are detected by a dedicated differential refractive index detector within an integrated temperature-controlled system to quantify the components and determine the polymer's molecular weight and its distribution. The mobile phase consisted of chromatographic-grade water (H_2O) or N,N-dimethylformamide (DMF). The sample was dissolved in the solvent at a concentration of 5 mg/mL, filtered through a 0.22 μm filter, and then injected for analysis.

Nuclear Magnetic Resonance Spectroscopy (NMR)

^1H NMR, ^{13}C NMR, and ^{31}P NMR spectra of the starting materials and products were recorded on a Bruker Avance 400 MHz spectrometer at 298 K. Deuterated chloroform ($CDCl_3$) or dimethyl sulfoxide (DMSO) was used as the solvent, with tetramethylsilane (TMS) as the internal standard. The molecular structure of the polymers was

investigated by analyzing the characteristic chemical shifts, peak shapes, and intensities in the spectra.

Fourier Transform Infrared Spectroscopy (FT-IR)

Fourier Transform Infrared Spectroscopy is a common technique for identifying functional groups in polymers. The testing procedure is as follows: for liquid samples, an appropriate amount was directly placed on the testing window. For solid samples, the material was ground into a powder before being placed on the window. The spectra were obtained using an FTIR-IS50 spectrometer by scanning the samples over a wavenumber range of 4000 to 400 cm^{-1} with 32 scans. The resulting data was processed to generate the infrared spectrum.

Ultraviolet-Visible Absorption Spectroscopy (UV)

The ultraviolet-visible absorption spectra of polymer solutions at various concentrations were measured at room temperature using a U-3900 UV-Vis spectrophotometer. The scanning range was 200-800 nm with a sampling interval of 0.5 nm. The testing method involved loading the sample solution and a reference (pure solvent) into separate micro quartz cuvettes, which were then placed inside the spectrophotometer to obtain the absorption spectra.

Photoluminescence Spectroscopy (PL)

The excitation and emission spectra of polymer solutions under different conditions were measured at room temperature using a Hitachi F-4600 fluorescence spectrophotometer. The instrument is equipped with a xenon lamp light source and covers a wavelength scanning range of 200-800 nm. The testing procedure consisted of placing the sample solution in a quartz cuvette inside the spectrophotometer. The excitation spectra, emission spectra, and 3D fluorescence spectra were then acquired by adjusting instrument parameters such as slit width and photomultiplier tube voltage.

Fluorescence Quantum Yield (QY)

The absolute fluorescence quantum yield of the polymers was measured using an Edinburgh Instruments FLS980 steady-state/transient fluorescence spectrometer (UK) equipped with an integrating sphere. The fluorescence quantum yield refers to the

percentage of excited molecules that emit fluorescence among all excited molecules and is denoted as QY.

Fluorescence Lifetime (τ)

The fluorescence lifetime of the polymers was measured using an Edinburgh Instruments FLS1000 steady-state and transient fluorescence spectrometer. Fluorescence lifetime is defined as the time required for the fluorescence emission intensity to decay from its maximum value I_0 to I_0/e after the molecules are excited by an external energy source. The fluorescence decay curves were fitted using the software provided with the instrument.

Synthesis of polyphosphate (LPPE)

LPPE was synthesized via a one-step transesterification polycondensation reaction using dimethyl phosphite (DMP) and diethylene glycol (DEG) as starting materials. The molar ratio of DMP to DEG was designed to be 1:1.1, corresponding to an equivalent ratio of phosphite ester groups to hydroxyl groups of 1:1.1. At room temperature, DMP (22.01 g, 0.2 mol) and DEG (23.35 g, 0.22 mol) were added to a 250 mL three-neck flask equipped with a thermometer, a stir bar, a nitrogen inlet, and a condenser. The mixture was stirred thoroughly to ensure homogeneity. The temperature was then gradually increased until methanol began to distill off as a by-product. The reaction mixture was heated slowly to 120°C and maintained at this temperature for 5 hours, while keeping the distillation temperature below 45°C. After the reaction, heating was stopped and the system was allowed to cool to room temperature, yielding crude product. A transparent product was obtained, and the distillate was collected. The crude product was transferred to a 100 mL beaker and dissolved in a suitable amount of ethanol until a clear, transparent solution was achieved. This solution was transferred into a dialysis bag (molecular weight cut-off: 1000 Da) and sealed with clips. The dialysis bag was immersed in a 1000 mL beaker filled with a large volume of anhydrous ethanol, ensuring the bag was completely submerged. The beaker was sealed with plastic film, and dialysis was performed for 24 hours. Upon completion, a colorless, transparent liquid was obtained inside the dialysis bag. This liquid was poured into a

pear-shaped flask, and the ethanol was removed using a rotary evaporator. The residual liquid in the flask was then placed in a vacuum drying oven, sealed with plastic film, and dried for 3 hours to remove any remaining ethanol completely, resulting in high-purity LPPE.

Synthesis of N-salicylidene-butylamine (Schiff 1)

At room temperature, 1.1 g (9 mmol) of salicylaldehyde and 0.658 g (9 mmol) of n-butylamine were added to a 100 mL single-neck flask containing 50 mL of dichloroethane. The reaction mixture was stirred at room temperature for 14 h. After the reaction, the solvent was removed by reduced-pressure distillation, and the resulting product was further dried under vacuum to eliminate any residual water, yielding a yellow oily product (1.55 g). The spectral data were consistent with those reported in the literature[1].

^{1}H NMR (400MHz, Chloroform-d) δ13.63 (s, 1H, OH), 8.26 (s, 1H, CHN), 7.26–7.13 (m, 2H, aromaticCH), 6.88 (d, J=8.3Hz, 1H, aromaticCH), 6.79 (td, J=7.5, 1.1Hz, 1H, aromaticCH), 3.52 (td, J=6.8, 1.2Hz, 2H, CH_2), 1.61 (p, J=7.0Hz, 2H, CH_2), 1.34 (h, J=7.4Hz, 2H, CH_2), 0.88 (t, J=7.4Hz, 3H, CH_3).

^{13}C NMR (101MHz, DMSO-d_6) δ166.08 (C=N), 161.36 (C-OH), 132.60 (C-H), 131.98 (C-H), 119.04 (C-H), 118.79 (C-H), 116.94 (C-H), 58.36 (CH_2), 32.90 (CH_2), 20.22 (CH_2), 14.07 (CH_3).

Synthesis of N,N'-bis-(2-hydroxybenzylidene)benzene-1,4-diamine (Schiff 2)

At room temperature, 1.1 g (9 mmol) of salicylaldehyde and 0.487 g (4.5 mmol) of 1,4-phenylenediamine were added to a 100 mL single-neck flask containing 50 mL of methanol. The mixture was stirred under reflux for 30 min, then cooled to room temperature. The resulting solid was collected by filtration, washed with methanol, and dried under vacuum to afford an orange powder (1.4 g). The spectral data were consistent with those reported in the literature[2].

^{1}H NMR (400 MHz, DMSO-d6) δ13.08 (s, 1H, OH), 9.04 (s, 1H, CHN), 7.68 (d, J=7.6Hz, 1H, aromaticCH), 7.55 (s, 2H, aromaticCH), 7.47–7.39 (m, 1H, aromaticCH), 7.00 (dd, J=10.8, 7.9Hz, 2H, aromaticCH).

^{13}C NMR (101MHz, DMSO-d_6) δ163.63 (C=N), 160.79 (C-OH), 147.16 (C-H), 133.83 (C-H), 133.03 (C-H), 123.04 (C-H), 119.85 (C-H), 119.66 (C-H), 117.10 (C-H).

The synthesis processes of Schiff-1 and Schiff 2 are depicted in the figure S1.

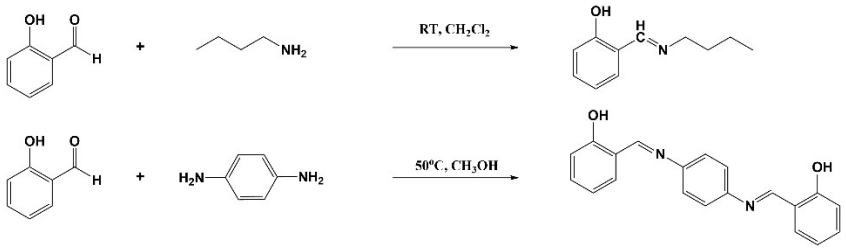

Figure S1. Synthesis route of Schiff 1, Schiff 2

Synthesis of LPPE-αAPB

Using the synthesized Schiff 2 and LPPE as starting materials, α-aminophosphonate-bridged polyphosphonate LPPE-αAPB was synthesized via a one-step Kabachnik–Fields reaction, with a designed molar ratio of polymer repeating unit to Schiff base of 1:0.25. At room temperature, a stir bar and 50 mL of anhydrous methanol were added to a single-neck flask, followed by 1.304 g of Schiff 2, resulting in a yellow turbid mixture. After adding 5.01 g of the polymer LPPE, the bottom of the mixture turned red. The reaction was stirred under reflux for 12 h, during which the mixture gradually changed into a clear claret-red solution. The solution was transferred to a pear-shaped flask, and methanol was removed using a rotary evaporator. The remaining liquid was placed in a vacuum drying oven and dried overnight to remove residual methanol, yielding high-purity α-aminophosphonate-bridged polyphosphonate LPPE-αAPB.

The synthesis process of LPPE-αAPB is depicted in the figure S2.

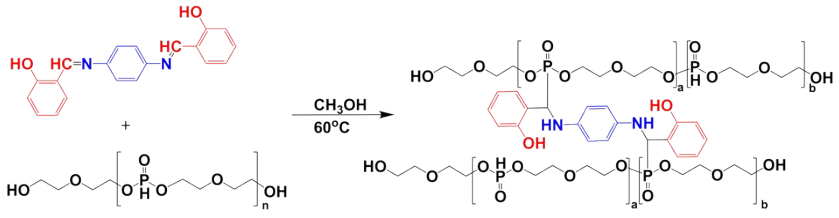

Figure S2. The synthesis process of LPPE-αAPB

Synthesis of LPPE-αAP

LPPE-αAP was synthesized using a method analogous to that of LPPE-αAPB. For the preparation of LPPE-αAP, 1.46 g of Schiff-2 and 5.01 g of the polymer LPPE were

employed as starting materials. Following reaction, purification via dialysis, concentration by rotary evaporation, and drying under vacuum yielded high-purity α-aminophosphonate-unbridged polyphosphonate LPPE-αAP.

The synthesis process of LPPE-αAP is depicted in the figure S3.

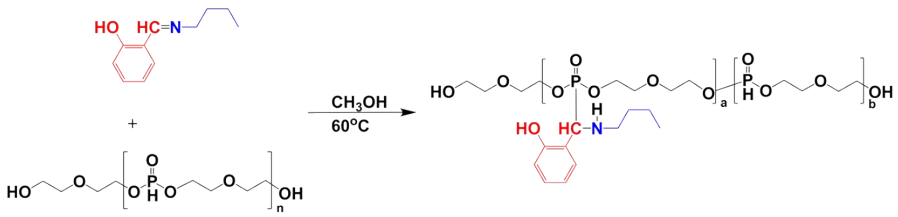

Figure S3. The synthesis process of LPPE-αAP

Metal Ion Responsiveness

(1) Preparation of LPPE-αAPB Aqueous Solutions Containing Different Metal Ions

0.5 g of LPPE-αAPB was dissolved in deionized water and brought to volume in a 50 mL volumetric flask. Then, 10 aliquots of 2.5 mL each of the prepared LPPE-αAPB aqueous solution (10 mg/mL) were measured out. To each aliquot, 0.05 mL of a solution containing Co^{2+}, Na^{+}, Ca^{2+}, Al^{3+}, Zn^{2+}, Cu^{2+}, Fe^{3+}, Ba^{2+}, Hg^{2+}, or Cd^{2+} (10^{-2} M) was added separately. Each mixture was then diluted to a final volume of 5 mL with deionized water.

(2) Preparation of LPPE-αAPB Aqueous Solutions Containing Different Concentrations of Metal Ions

16 aliquots of 2.5 mL each of the prepared LPPE-αAPB aqueous solution (5 mg/mL) were measured out. Different volumes and concentrations of Cu^{2+} solution were added to prepare ion solutions with the following final concentrations: 0, 2×10^{-6}, 4×10^{-6}, 6×10^{-6}, 8×10^{-6}, 1×10^{-5}, 2×10^{-5}, 4×10^{-5}, 6×10^{-5}, 8×10^{-5}, 1×10^{-4}, 2×10^{-4}, 4×10^{-4}, 6×10^{-4}, 8×10^{-4}, 1×10^{-3} M.

6 aliquots of 2.5 mL each of the prepared LPPE-αAPB aqueous solution (5 mg/mL) were measured out. Different volumes and concentrations of Hg^{2+} solution were added to prepare ion solutions with the following final concentrations: 1×10^{-4}, 2×10^{-4}, 4×10^{-4}, 6×10^{-4}, 8×10^{-4}, 1×10^{-3} M.

6 aliquots of 2.5 mL each of the prepared LPPE-αAPB aqueous solution (5 mg/mL)

were measured out. Different volumes and concentrations of Fe^{3+} solution were added to prepare ion solutions with the following final concentrations: 1×10^{-4}, 2×10^{-4}, 4×10^{-4}, 6×10^{-4}, 8×10^{-4}, 1×10^{-3} M.

Results and Discussion

Analysis of the NMR Spectra of LPPE

The ^{1}H NMR spectra of the starting materials DEG and DMP are shown in Figure S4 A, and the ^{1}H NMR spectrum of the product LPPE is shown in Figure S4 B.

In the ^{1}H NMR spectrum of DMP, the signal at δ = 3.67 ppm is assigned to the O–C$\underline{H}_3$ protons. The signals at δ = 7.64 ppm and 5.90 ppm, which appear as split peaks due to coupling with phosphorus, are attributed to the P–$\underline{H}$ proton.

In the ^{1}H NMR spectrum of DEG, two characteristic signals are observed. The signal at δ = 7.28 ppm corresponds to the O–$\underline{H}$ proton, while the signals at δ = 3.75 ppm and 3.62 ppm are assigned to the –O–C$\underline{H}_2$–C$\underline{H}_2$–O–H protons.

In the ^{1}H NMR spectrum of the product obtained from the reaction between DEG and DMP, peak 6, corresponding to the P–$\underline{H}$ proton, is observed at δ = 6.04 ppm and 7.84 ppm, which is essentially consistent with its chemical shift before the reaction. Peak 3, corresponding to the terminal O–C$\underline{H}_3$ protons, appears at δ = 3.65 ppm, also largely unchanged from its pre-reposition position. Peaks 1 and 2, assigned to the –O=P–O–C$\underline{H}_2$–C$\underline{H}_2$–O– protons, shift downfield due to the influence of the phosphate ester group, appearing at δ = 4.01 ppm and 4.13 ppm, respectively. Peaks 4 and 5, assigned to the –O–C$\underline{H}_2$–C$\underline{H}_2$–O–H protons, appear at δ = 3.43 ppm. Peak 7, corresponding to the –O$\underline{H}$ proton, is observed at δ = 5.24 ppm.

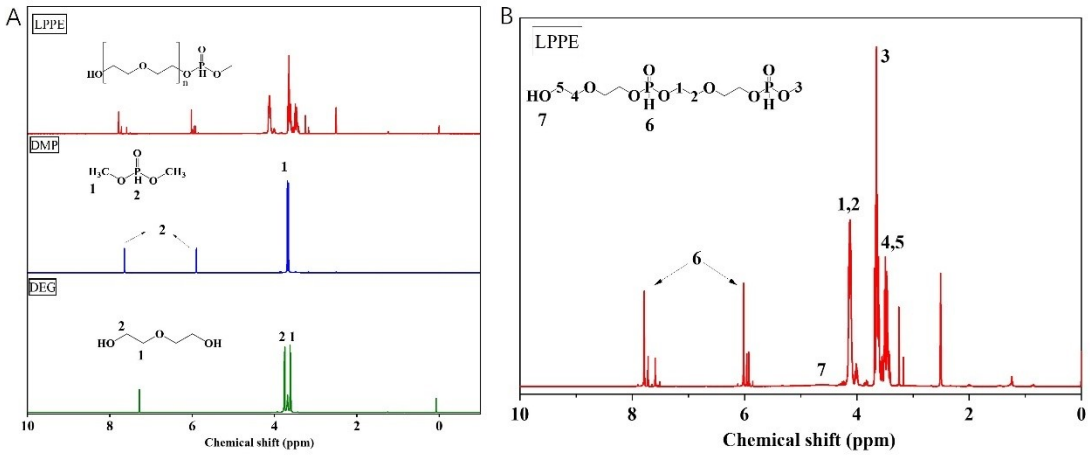

Figure S4. (A) ^{1}H NMR spectral of DMP, DEA, LPPE; (B) ^{1}H NMR of LPPE

The ^{13}C NMR spectra of the starting materials DEG, DMP, and the product LPPE are shown in Figure S5 A, while the ^{31}P NMR spectra of DMP and LPPE are shown in Figure S5 B.

In the ^{13}C NMR spectrum of DEG, peak 1 is assigned to O–CH_2–$\underline{C}H_2$–OH at δ = 61.49 ppm, and peak 2 is assigned to O–$\underline{C}H_2$–CH_2–OH at δ = 72.34 ppm. In the ^{13}C NMR spectrum of DMP, the signal is assigned to O–$\underline{C}H_3$ at δ = 52.20 ppm. In the ^{13}C NMR spectrum of LPPE, peak 1 is assigned to O–CH_2–$\underline{C}H_2$–OH at δ = 60.61 ppm, and peak 2 is assigned to O–$\underline{C}H_2$–CH_2–OH at δ = 71.67 ppm, both of which are essentially consistent with the chemical shifts observed before the reaction. Peaks 3 and 5 are assigned to O–$\underline{C}H_2$–CH_2–O–P=O at δ = 70.04 ppm, peak 4 to O–CH_2–$\underline{C}H_2$–O–P=O at δ = 63.98 ppm, peak 6 to O–CH_2–$\underline{C}H_2$–O–P=O at δ = 64.79 ppm, and peak 7 to $\underline{C}H_3$–P=O at δ = 52.05 ppm. The appearance of C3, C4, C5, and C6 further confirms the successful synthesis of LPPE, while the retention of C7 indicates that a small amount of O–$\underline{C}H_3$ groups in LPPE remain unsubstituted by –OH.

From the ^{31}P NMR spectra, it can be seen that the phosphorus signal of the product shifts compared to that of the starting material DMP (δ = 11.94 ppm), appearing at δ = 6.47 ppm, 5.30 ppm, and 1.44 ppm, which indirectly confirms the formation of the product.

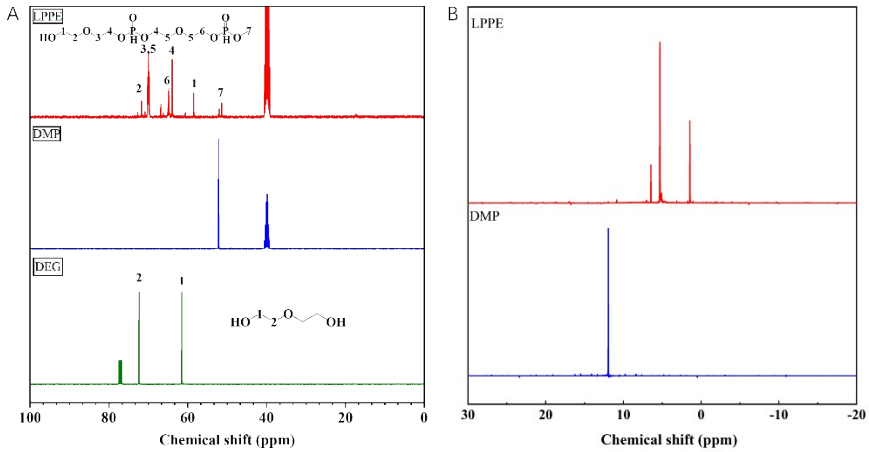

Figure S5. (A) ^{13}C NMR of DMP, DEA, LPPE; (B) ^{31}P NMR of DMP, LPPE

Analysis of the FTIR Spectra of LPPE

The infrared spectra of the raw materials DEG, DMP, and the polymer LPPE are shown in Figure S6.

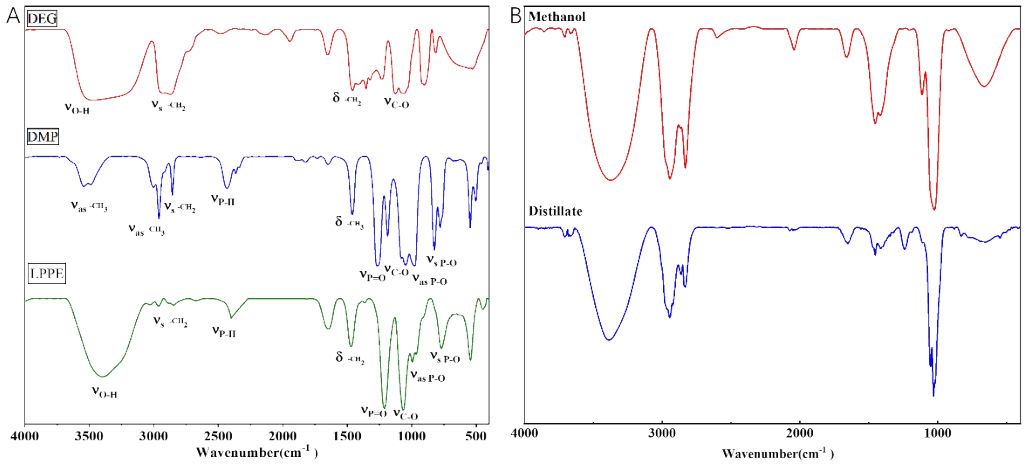

Figure S6. (A) FT-IR spectra of DEG, DMP and LPPE; (B) FT-IR spectra of distillate and standard methanol

From the infrared spectrum of DEG, the absorption peaks are assigned as follows: the broad absorption peak near 3507 cm^{-1} is attributed to the stretching vibration of the associated -OH group; the absorption peaks near 2948 cm^{-1} and 1465 cm^{-1} are assigned to the stretching and bending vibrations of the -CH_2- group, respectively; the peaks at 1128 cm^{-1} and 1062 cm^{-1} are assigned to the stretching vibrations of C-O and C-O-C, respectively. From the infrared spectrum of DMP, the absorption peaks are assigned as follows: the absorption peak at 1465 cm^{-1} and the peak near 3548 cm^{-1} are attributed to

the bending and stretching vibrations of the -CH_3 group, respectively; the absorption peak at 2958 cm^{-1} is assigned to the stretching vibration of the -CH_2- group; the absorption peak at 2428 cm^{-1} is attributed to the stretching vibration of P-H; the absorption peak at 1269 cm^{-1} is assigned to the stretching vibration of P=O; the absorption peak at 1043 cm^{-1} is attributed to the stretching vibration of C-O; and the absorption peaks at 975 cm^{-1} and 827 cm^{-1} are assigned to the stretching vibrations of P-O. By comparing the spectra of the raw materials DMP and DEG with that of the product LPPE, it can be observed that the characteristic groups in the main structure, such as P=O (1216 cm^{-1}), P-O (998 cm^{-1}, 775 cm^{-1}), C-O (1062 cm^{-1}), and -CH_2 (1471 cm^{-1}), show no significant changes. Notable differences, however, reveal a distinct hydroxyl peak (3403 cm^{-1}) in the LPPE spectrum, indicating that DMP and DEG have reacted and that the reaction is terminated by hydroxyl groups. Simultaneously, the presence of P-H (2402 cm^{-1}) suggests that phosphorus still exists in the form of phosphite ester.

Analysis of the NMR Spectra of LPPE-αAPB

The ^{1}H NMR spectra of the Schiff 1, LPPE and LPPE-αAPB are shown in Figure S7.

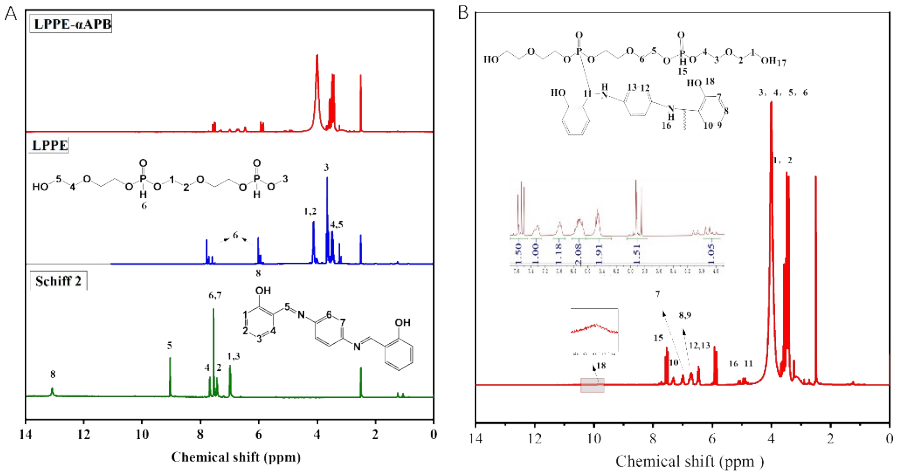

Figure S7. (A) ^{1}H NMR spectra of Schiff 2, LPPE, LPPE-αAPB; (B) Detailed ^{1}H NMR spectral data of LPPE-αAPB

In the ^{1}H NMR spectrum of Schiff 2, peaks 1, 2, 3, 4, 6, and 7 are assigned to the aromatic protons, with chemical shifts around 7.0–7.7 ppm. Peak 5 corresponds to the –CH=N– proton at δ = 9.03 ppm, and peak 8 is attributed to the phenolic hydroxyl

proton at δ = 13.07 ppm. The peak assignments for LPPE are consistent with those described previously. In the ^{1}H NMR spectrum of LPPE-αAPB, compared with that of LPPE, peaks 1 and 2 are assigned to O–C<u>H</u>$_2$–C<u>H</u>$_2$–OH at δ = 3.42 ppm; peaks 3, 4, 5, and 6 correspond to O–C<u>H</u>$_2$–C<u>H</u>$_2$–O–P(=O)–O–C<u>H</u>$_2$–C<u>H</u>$_2$–O at δ = 4.01 ppm; and peak 15 is attributed to the unreacted P–<u>H</u> proton at δ = 5.91 ppm and 7.51 ppm. These signals remain largely unchanged from those before the reaction. Compared with the spectrum of Schiff 2, the –C<u>H</u>=N– peak completely disappears, and a newly formed –C<u>H</u>–NH– peak appears at δ = 4.89 ppm. Slight changes are observed in the aromatic proton signals: peaks 7, 8 (9), 10, and 12 (13) appear at δ = 7.00 ppm, 6.69 ppm, 7.31 ppm, and 6.47 ppm, respectively. Moreover, the integration ratios of peaks 15, 10, 7, 8 (9), 12 (13), and 11 are approximately 3.01 : 1.00 : 1.18 : 2.08 : 1.91 : 1.05, which closely align with the expected ratio of 3 : 1 : 1 : 2 : 2 : 1, confirming that the reaction proceeded as designed.

The ^{13}C NMR and ^{31}P NMR spectra of the raw materials and LPPE-αAPB are shown in Figure S8.

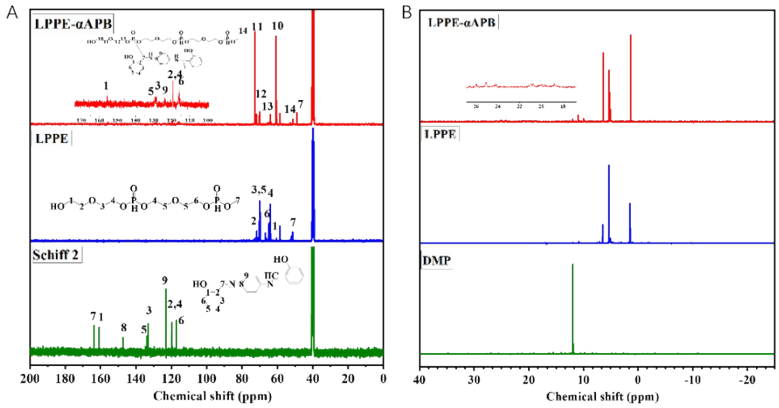

Figure S8. (A) ^{13}C NMR spectra of Schiff 2, LPPE, LPPE-αAPB; (B) ^{31}P NMR spectra of DMP, LPPE-αAPB

In the ^{13}C NMR spectrum of Schiff 2, peak 7 is assigned to the <u>C</u>=N carbon at δ = 163.63 ppm. Peak 1 is assigned to the carbon ortho to the phenolic hydroxyl group at δ = 160.79 ppm. Peaks 2 (4), 3, 5, 6, 8, and 9 correspond to the aromatic carbons of the benzene ring, with chemical shifts approximately in the range of 110–147 ppm. The assignments for the ^{13}C NMR spectrum of LPPE remain consistent with those previously described. In the ^{13}C NMR spectrum of LPPE-αAPB, compared to that of LPPE, peak 10 is assigned to O–CH$_2$–<u>C</u>H$_2$–OH at δ = 60.71 ppm, and peak 11 is

assigned to O–C̲H₂–CH₂–OH at δ = 72.74 ppm. These chemical shifts are essentially unchanged from before the reaction, but their relative intensities are significantly increased. This is attributed to the ongoing alcoholysis of the Polyphosphate during the grafting reaction, leading to a continuous increase in terminal diethylene glycol segments. Peak 12 is assigned to O–C̲H₂–CH₂–O–P=O at δ = 70.01 ppm, peak 13 to O–CH₂–C̲H₂–O–P=O at δ = 63.99 ppm, and peak 14 to C̲H₃–P=O at δ = 51.35 ppm, with their chemical shifts largely consistent with the pre-reaction values. Compared to the ^{13}C NMR spectrum of Schiff 2, the C=N peak has completely disappeared. A newly formed –C̲H–NH– carbon appears at δ = 49.08 ppm. The chemical shift of the carbon ortho to the phenolic hydroxyl group is δ = 156.24 ppm, which is essentially unchanged from before the reaction. The chemical shifts of the remaining aromatic carbons show minimal variation.

From the ^{31}P NMR spectrum, it is evident that the phosphorus signals of the product have shifted compared to those of LPPE (δ = 6.47 ppm, 5.30 ppm, 1.44 ppm). New peaks appear around 20 ppm and 24 ppm, which are assigned to O=P̲–C, indirectly confirming the successful synthesis of the product.

Analysis of the NMR Spectra of LPPE-αAP

The ^{1}H NMR spectra of the Schiff 1, LPPE and LPPE-αAP are shown in Figure S9.

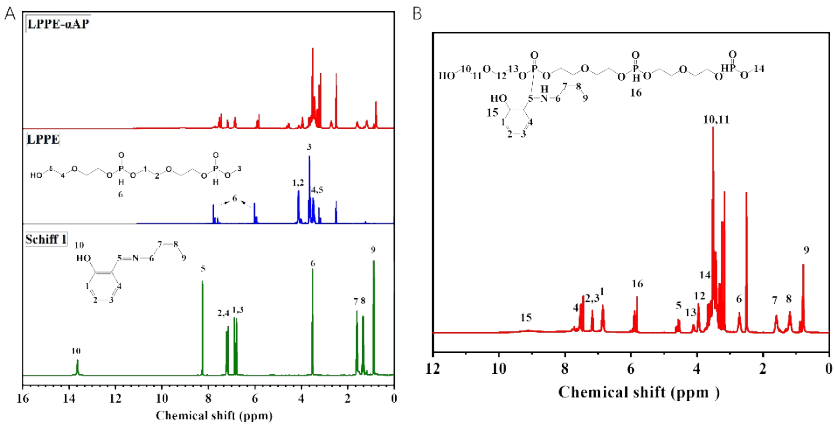

Figure S9. (A) ^{1}H NMR spectra of Schiff 1, LPPE, LPPE-αAP; (B) Detailed ^{1}H NMR spectral data of LPPE-αAP

In the ^{1}H NMR spectrum of Schiff 1, peaks 1, 2, 3, and 4 are assigned to the aromatic

protons, with chemical shifts in the range of approximately 6.7–7.2 ppm. Peak 5 corresponds to the –C<u>H</u>=N– proton at δ = 8.26 ppm, peak 10 is attributed to the phenolic hydroxyl proton at δ = 13.64 ppm, and peak 6 is assigned to the C=N–C<u>H</u>$_2$–CH$_2$–CH$_2$–CH$_3$ protons at δ = 3.51 ppm. Peaks 7, 8, and 9 correspond to the remaining methylene and methyl protons of the butyl chain (C=N–CH$_2$–C<u>H</u>$_2$–C<u>H</u>$_2$–C<u>H</u>$_3$) at δ = 1.61 ppm, 1.33 ppm, and 0.89 ppm, respectively.

The ^{1}H NMR spectral assignments for LPPE are as previously described. Compared to the spectrum of LPPE, peaks 10 and 11 in the LPPE-αAP spectrum are assigned to O–C<u>H</u>$_2$–C<u>H</u>$_2$–OH at δ = 3.46 ppm; peaks 12 and 13 correspond to O–C<u>H</u>$_2$–C<u>H</u>$_2$–O–P=O at δ = 3.95 ppm and 4.13 ppm; peak 16 is attributed to the unreacted P–<u>H</u> proton at δ = 5.82 ppm and 7.44 ppm; and peak 14 corresponds to the terminal methoxy group P–OC<u>H</u>$_3$ at δ = 3.65 ppm. These signals remain largely consistent with those observed prior to the reaction. In comparison with the ^{1}H NMR spectrum of Schiff 1, the –C<u>H</u>=N– peak has completely disappeared. A newly formed –C<u>H</u>–NH– peak appears at δ = 4.60 ppm. Correspondingly, the signals for the n-butyl chain shift upfield and are observed at δ = 2.74 ppm, 1.60 ppm, 1.18 ppm, and 0.78 ppm, with an integration ratio of approximately 1:1:1:1.5. Slight changes are also noted in the aromatic proton signals: peaks 1, 2 (3), and 4 appear at δ = 6.85 ppm, 7.18 ppm, and 7.53 ppm, respectively. These observations collectively confirm that the reaction proceeded essentially as designed.

The ^{13}C NMR and ^{31}P NMR spectra of the raw materials and LPPE-αAP are shown in Figure S10.

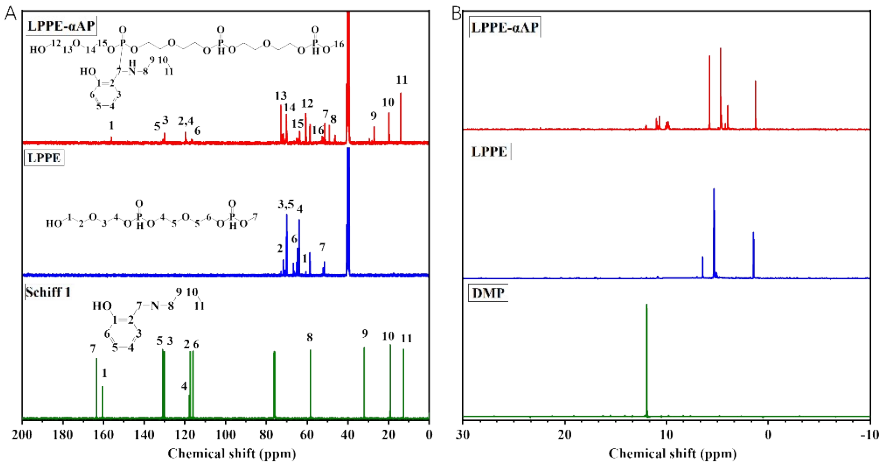

Figure S10. (A) ^{13}C NMR spectral of Schiff 1, LPPE, LPPE-αAP; (B) ^{31}P NMR spectral of DMP, LPPE-αAP

In the ^{13}C NMR spectrum of Schiff 1, peak 7 is assigned to the C=N carbon at δ = 163.41 ppm. Peak 1 corresponds to the carbon ortho to the phenolic hydroxyl group at δ = 160.37 ppm. Peaks 2, 3, 4, 5, and 6 are attributed to the aromatic carbons of the benzene ring, with chemical shifts approximately in the range of 116–130 ppm. The signals for the butyl chain are assigned as follows: peak 8 (C=N–$\underline{C}H_2$–) at δ = 58.17 ppm, peak 9 (C=N–CH_2–$\underline{C}H_2$–CH_2–CH_3) at δ = 31.88 ppm, peak 10 (C=N–CH_2–CH_2–$\underline{C}H_2$–CH_3) at δ = 19.26 ppm, and peak 11 (–CH_3) at δ = 12.75 ppm. The ^{13}C NMR spectral assignments for LPPE are consistent with those previously described. In the spectrum of LPPE-αAP, compared to that of LPPE, peaks 12 and 13 are assigned to O–$\underline{C}H_2$–$\underline{C}H_2$–OH at δ = 60.71 ppm and δ = 72.74 ppm, respectively. Their chemical shifts remain largely unchanged; however, a significant increase in their relative intensity is observed. This is attributed to the ongoing alcoholysis of the polyphosphonate during the grafting reaction, leading to a continuous increase in terminal diethylene glycol segments. Peaks 14 and 15 correspond to O–$\underline{C}H_2$–CH_2–OP=O at δ = 70.20 ppm and δ = 63.76 ppm, respectively. Peak 16 is assigned to $\underline{C}H_3$–P=O at δ = 52.26 ppm, with chemical shifts essentially consistent with pre-reaction values. Compared to the ^{13}C NMR spectrum of Schiff 1, the C=N peak (δ = 163.41 ppm) is completely absent. A newly formed –$\underline{C}$H–NH– carbon signal appears at δ = 51.20 ppm. Correspondingly, the signals for the butyl chain shift upfield: the C=N–$\underline{C}H_2$– carbon (peak 8) is observed at

δ = 49.05 ppm, the C=N–CH_2–$\underline{C}H_2$–CH_2–CH_3 carbon (peak 9) at δ = 27.03 ppm, the –C=N–CH_2–CH_2–$\underline{C}H_2$–CH_3 carbon (peak 10) at δ = 19.80 ppm, and the terminal –$\underline{C}H_3$ carbon (peak 11) at δ = 13.92 ppm. The chemical shift of the carbon ortho to the phenolic hydroxyl group is δ = 156.24 ppm, which is essentially unchanged from its position prior to the reaction, while the chemical shifts of the remaining aromatic carbons show minimal variation.

From the ^{31}P NMR spectrum, it is evident that the phosphorus signals of the product have shifted compared to those of LPPE (δ = 6.47, 5.30, 1.44 ppm). A new peak appears at approximately δ = 10 ppm, which is assigned to O=$\underline{P}$–C, indirectly confirming the successful synthesis of the product.

Analysis of the FTIR Spectra of LPPE-αAPB and LPPE-αAP

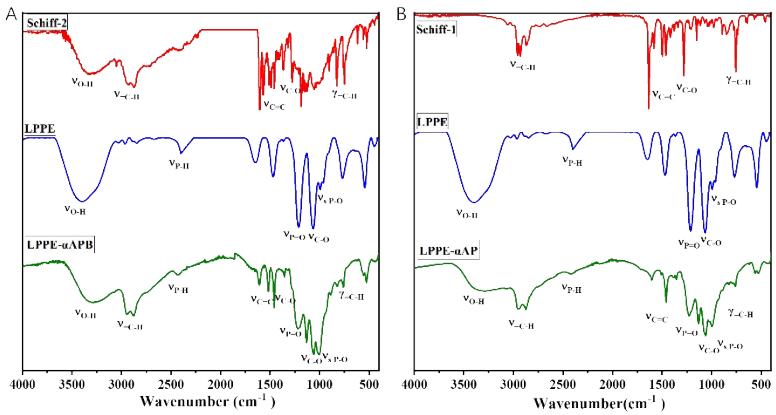

Figure S11. (A) FT-IR spectra of Schiff 2, LPPE, LPPE-αAPB; (B) FT-IR spectra of Schiff 1, LPPE, LPPE-αAP

From the infrared spectrum of Schiff 2, the absorption peaks are assigned as follows: the broad absorption peak near 3335 cm^{-1} is attributed to the O–H stretching vibration in the associated state; the peak at 1658 cm^{-1} is assigned to the N–H bending vibration; the absorption peaks near 2931 cm^{-1} and 2872 cm^{-1} correspond to the =C–H stretching vibrations on the benzene rings; the peaks at 1608 cm^{-1}, 1568 cm^{-1}, 1488 cm^{-1}, and 1457 cm^{-1} are assigned to the C=C stretching vibrations of the benzene rings; the peak at 1276 cm^{-1} corresponds to the C–O stretching vibration; the peaks at 827 cm^{-1} and 747 cm^{-1} are attributed to the out-of-plane bending vibrations of =C–H on the two

benzene rings, indicating that the benzene rings are meta-disubstituted and ortho-disubstituted, respectively. From the infrared spectrum of Schiff 1, the absorption peaks are assigned as follows: the absorption peaks near 2958 cm^{-1} and 2928 cm^{-1} are attributed to the =C–H stretching vibrations on the benzene ring; the peaks at 1631 cm^{-1}, 1583 cm^{-1}, 1496 cm^{-1}, and 1459 cm^{-1} correspond to the C=C stretching vibrations of the benzene ring; the peak at 1280 cm^{-1} is assigned to the C–O stretching vibration; the peak at 754 cm^{-1} corresponds to the out-of-plane bending vibration of =C–H on the benzene ring, indicating that the benzene ring is ortho-disubstituted. The infrared spectral assignments for LPPE are consistent with the previous analysis. By comparing the spectra of the starting material LPPE with that of the product LPPE-αAPB, it can be observed that the characteristic groups in the main structure, such as P=O (1219 cm^{-1}), P–O (1007 cm^{-1}), C–O (1063 cm^{-1}), and P–H (2402 cm^{-1}), show no significant changes, and the –OH group (3318 cm^{-1}) is still present. Meanwhile, the characteristic benzene ring functional groups from Schiff 2, C=C (1608 cm^{-1}, 1517 cm^{-1}, 1456 cm^{-1}) and =C–H (2952 cm^{-1}, 2857 cm^{-1}), appear. The out-of-plane bending vibration peaks of =C–H (822 cm^{-1}, 762 cm^{-1}) indicate that the substitution pattern of the benzene rings remains unchanged. By comparing the spectra of the starting material LPPE with that of the product LPPE-αAP, it is found that the characteristic groups in the main structure, including P=O (1225 cm^{-1}), P–O (997 cm^{-1}), C–O (1065 cm^{-1}), and P–H (2417 cm^{-1}), exhibit no significant changes, and the –OH group (3369 cm^{-1}) is still retained. Meanwhile, the characteristic benzene ring functional groups from Schiff 1, C=C (1607 cm^{-1}, 1460 cm^{-1}) and =C–H (2959 cm^{-1}, 2878 cm^{-1}), appear. The out-of-plane bending vibration peak of =C–H (762 cm^{-1}) indicates that the substitution pattern of the benzene ring remains unchanged.

Analysis of the GPC data of LPPE, LPPE-αAPB and LPPE-αAP

The molecular weights and their distributions of LPPE, LPPE-αAPB, and LPPE-αAP are shown in Figure S12 and Table S2.

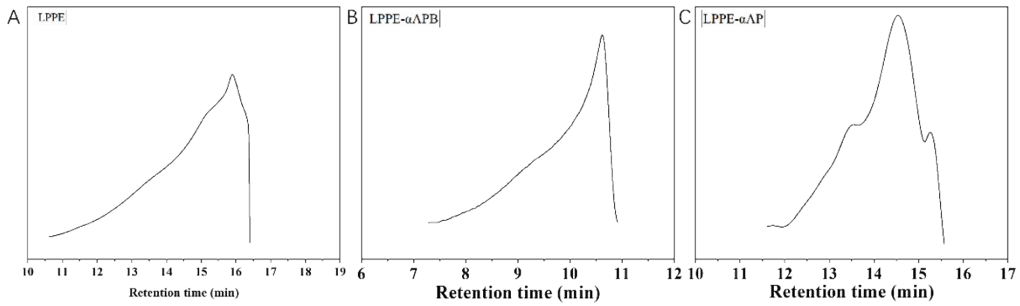

Figure S12. (A) GPC curve of LPPE; (B) GPC curve of LPPE-αAPB; (C) GPC curve of LPPE-αAP

As can be seen from the curves, LPPE elutes at approximately 15 min, with a number-average molecular weight (M_n) of 21,500. The synthesized LPPE exhibits a relatively broad molecular weight distribution, with a polydispersity index (PDI) of 3.03. LPPE-αAPB elutes at around 10 min (using DMF as the mobile phase), while LPPE-αAP elutes at approximately 14 min (using water as the mobile phase). The number-average molecular weights of LPPE-αAPB and LPPE-αAP are 26,700 and 25,300, respectively, which are relatively close to each other. It is worth noting that the molecular weights of the polyphosphonates modified with Schiff bases show a decrease compared to the unmodified precursor. This is attributed to the ongoing alcoholysis of the polyphosphonate in the methanol solution during the reaction, leading to a reduction in the degree of polymerization.

Table S2 Molecular weight and distribution of LPPE, LPPE-αAPB, and LPPE-αAP

Polymer	M_n	M_w	PDI
LPPE	21500	65400	3.03
LPPE-αAPB	26700	34400	1.29
LPPE-αAP	25300	29900	1.18

Quantum Yields and Fluorescence Lifetimes of LPPE, LPPE-αAP, and LPPE-αAPB

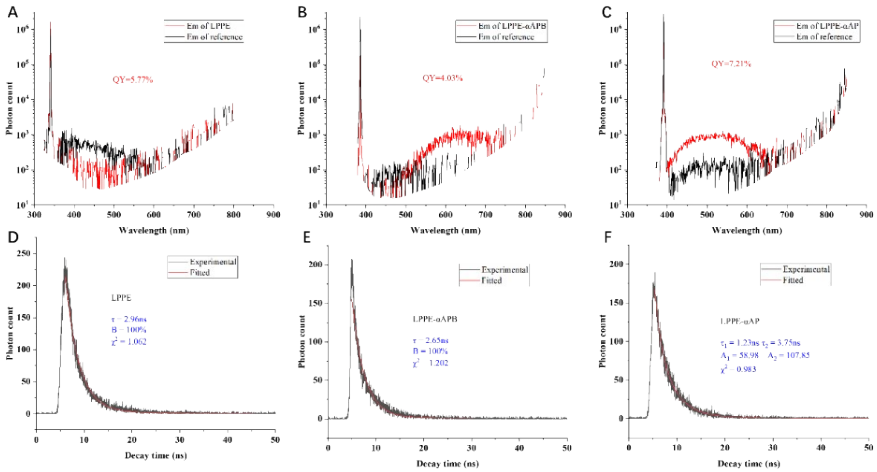

Figure S13. Quantum yields and fluorescence lifetimes of LPPE (A, D), LPPE-APB (B, E), and LPPE-αAP (C, F)

UV-Vis Absorption Spectra of LPPE, LPPE-αAP, and LPPE-αAP

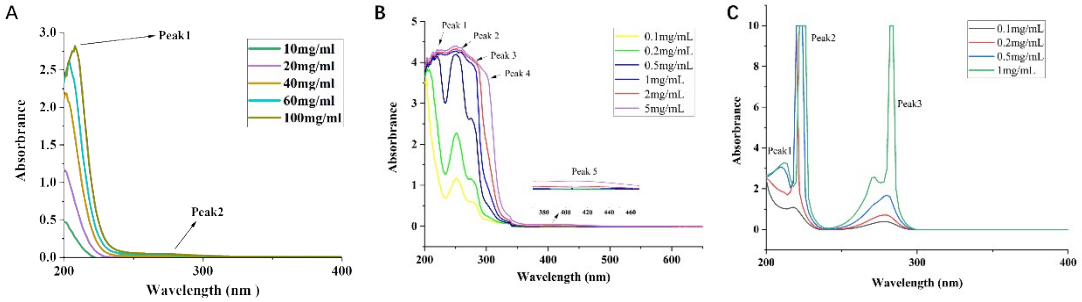

Figure S14. UV-Vis absorption spectra of LPPE (A, in ethanol), LPPE-αAPB (B, in aqueous solution), and LPPE-αAP (C, in aqueous solution) at various concentrations

AIEE characteristic of LPPE-αAPB

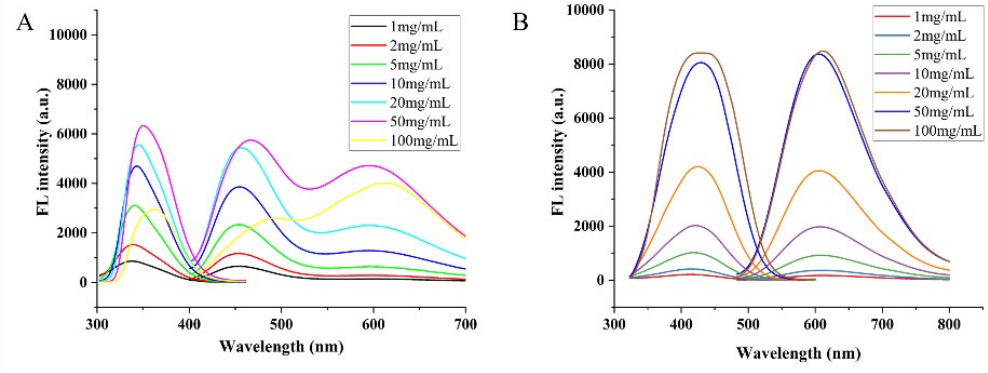

Figure S15. Fluorescence spectra of LPPE-αAPB at various concentrations under an excitation wavelength of 360 nm (A) and 430 nm (B)

AIE characteristic of LPPE-αAPB

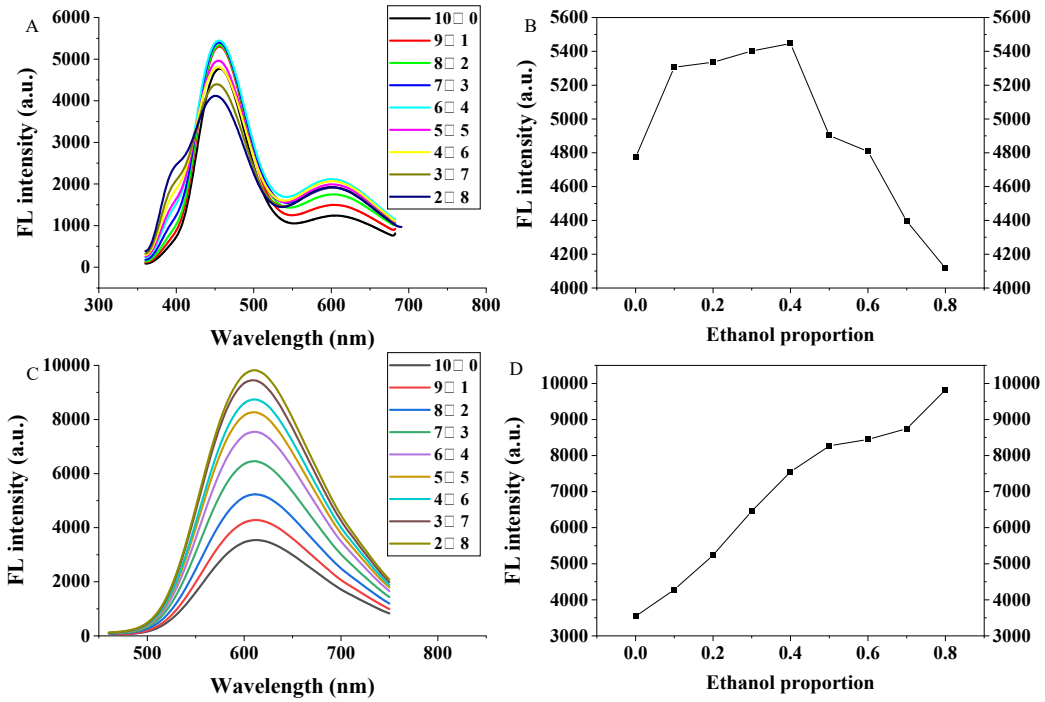

Figure S16. Fluorescence spectra of 10 mg/mL LPPE-α-APB solutions at varying ethanol fractions under 360 nm excitation (A) and the corresponding fluorescence intensity variation at the 460 nm emission peak (B); Fluorescence spectra under 410 nm excitation (C) and the corresponding fluorescence intensity variation at the 610 nm emission peak (D).

Analysis: The results indicate that under 360 nm excitation, the emission peak at 460 nm exhibits a slight blue-shift as the poor solvent fraction increases, with the intensity initially increasing and then decreasing, reaching its maximum at 40% ethanol content. In contrast, under 410 nm excitation, the emission peak at 610 nm remains virtually unchanged in position while the intensity continuously rises, reaching its maximum at 80% ethanol content. The general fluorescence enhancement is attributed to the increased proportion of the poor solvent, which strengthens intermolecular interactions and promotes the formation of aggregates; this restricts the motion of polymer segments, thereby reducing the energy dissipated through non-radiative pathways and increasing the radiative decay. Regarding the trend observed under 360 nm excitation where the 460 nm emission first increases and then decreases, the decline is likely due

to mechanisms similar to concentration quenching; furthermore, since there is a spectral overlap between the 460 nm emission and the 410 nm excitation peaks, the enhanced molecular aggregation induced by the poor solvent likely facilitates resonance energy transfer, leading to the sharp decline in the fluorescence emission intensity.

Fluorescence characteristic of Schiff 1 and Schiff 2

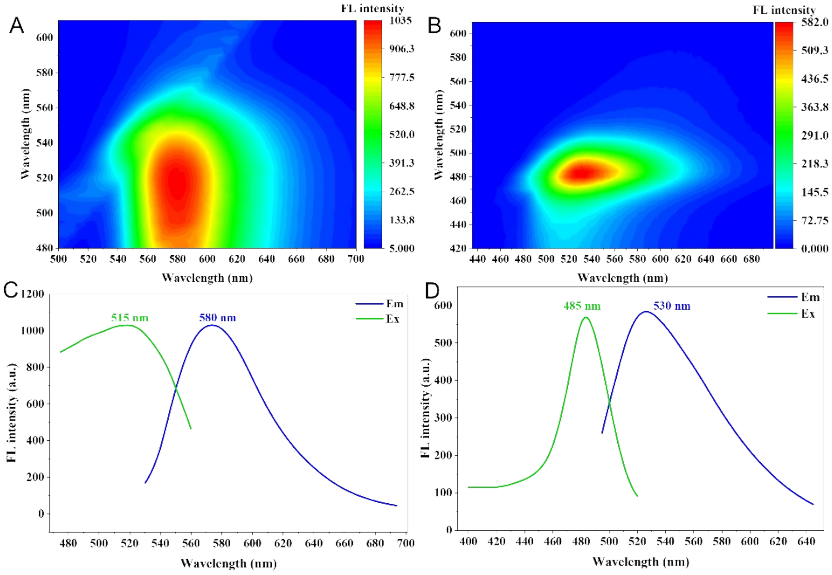

Figure S17. Excitation—emission matrix spectra and optimal excitation-emission spectra of Schiff 2 (A,C) and Schiff 1 (B,D)

Computational Molecular Model

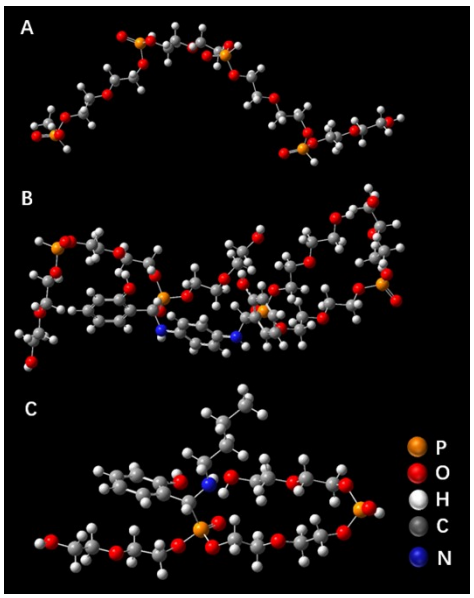

Figure S18. Computational Molecular Model: LPPE (A), LPPE-αAPB (B) , LPPE-αAP (C)

Schematic diagram of the optimized ground state structure of the two LPPE-αAPBs.

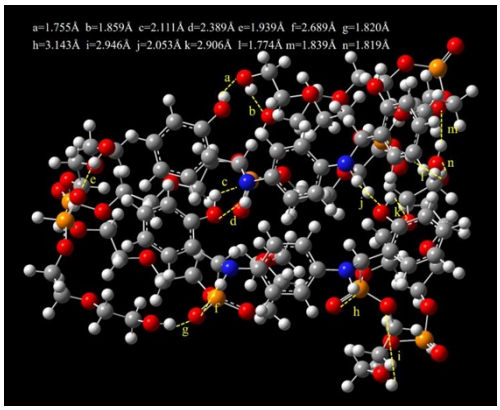

Figure S19. Schematic diagram of the optimized ground state structure of the two LPPE-αAPBs. The dotted line shows the intramolecular hydrogen bonding in the polymer

Excitation energy of LPPE and LPPE-αAPB simulated by TD-DFT

Table S3 Excitation energy of LPPE and LPPE-αAPB simulated by TD-DFT

Polymer	Excitation Energy（nm）	Oscillator Strengths	Orbital Excitation Composition
LPPE	173.50	0.0175	354-357
LPPE-αAPB	194.73	0.2486	295-304，298/299-307，301-317/319
	249.98	0.6147	301-307
LPPE-αAPB (2 moleculars)	252.50	0.6275	602-615，601-610，599-604
	264.10	0.1431	601-608

Schematic diagram of the orbital excitation composition of LPPE molecule simulated by TD-DFT

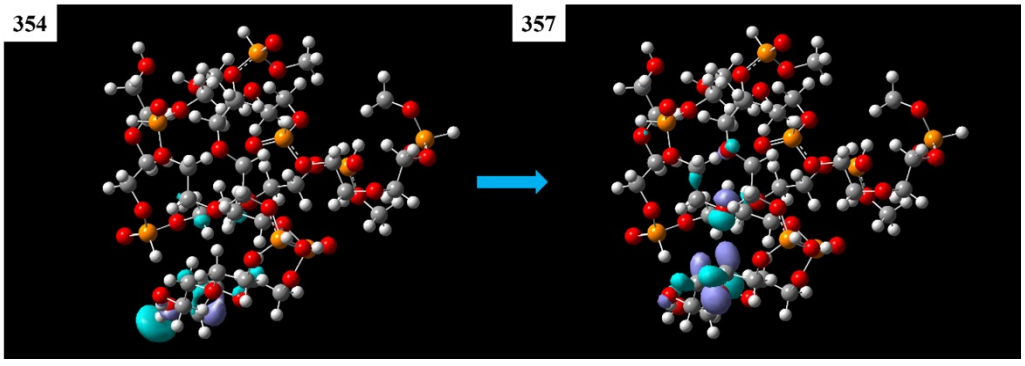

Figure S20. Schematic diagrams of the orbital excitation composition of a LPPE molecule simulated by TD-DFT. The white box means the molecular orbital number of this molecule.

Schematic diagram of the orbital excitation composition of LPPE-αAPB molecule simulated by TD-DFT

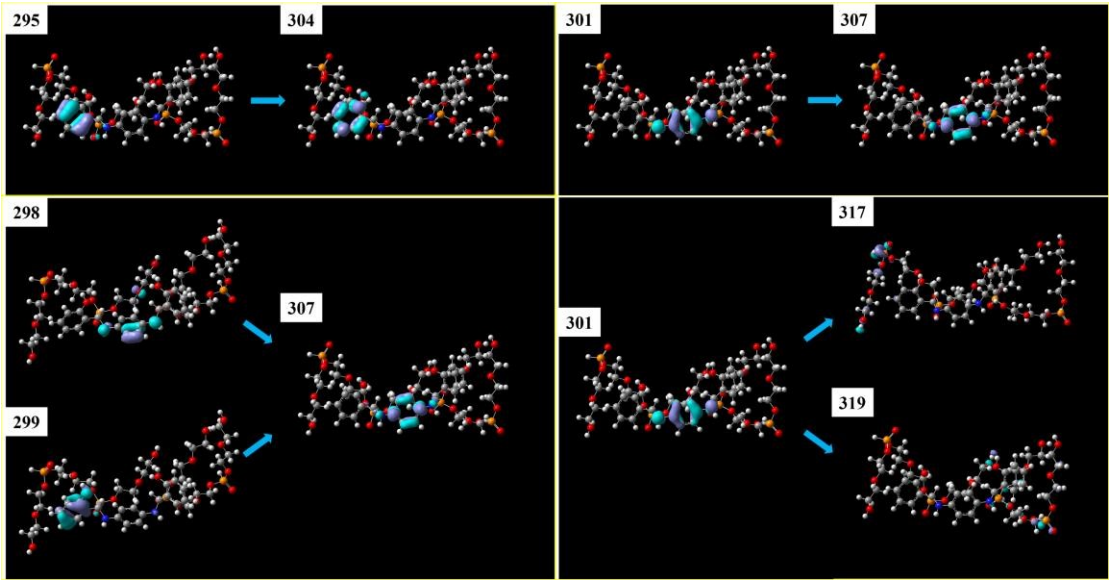

Figure S21. Schematic diagrams of the orbital excitation composition of a LPPE-αAPB molecule simulated by TD-DFT. The white box means the molecular orbital number of this molecule.

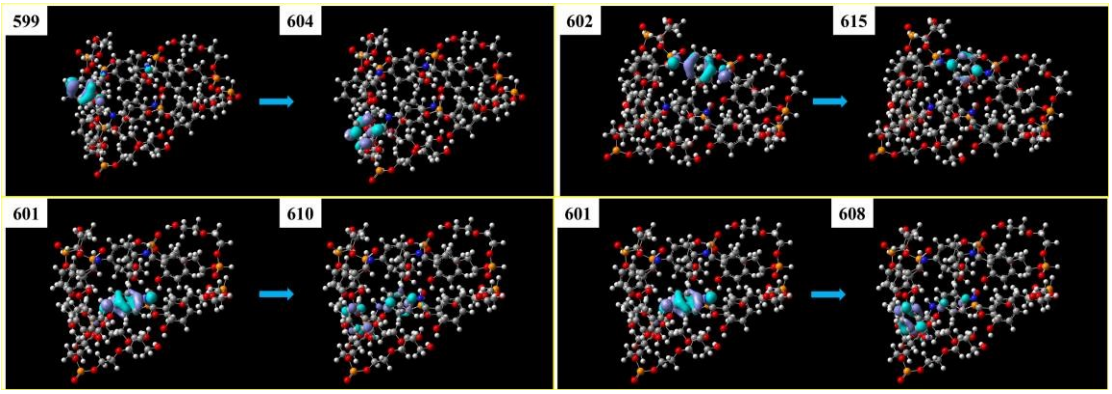

Figure S22. Schematic diagram of the orbital excitation composition of two LPPE-αAPB molecules simulated by TD-DFT. The white box means the molecular orbital number of this molecule.

Analysis：For a single LPPE-αAPB model molecule, at an excitation energy of 173.50 nm, the oscillator strength is f=0.2486. The major contributions to this excitation involve transitions from orbital 295 to 304, orbitals 298 and 299 to 307, and orbital 301 to 317 and 319. Orbitals 295, 299, and 304 are primarily distributed on the O=P-C-

PhOH segment; orbital 298 is mainly distributed on part of the benzene ring of the p-phenylenediamine moiety and the oxygen atoms of the spatially adjacent polyphosphate segments; orbital 301 is primarily distributed on the P-C-N-Ph-N segment; orbital 307 is primarily distributed on the O-P-C-N-Ph-N segment; orbital 317 is mainly distributed on the O=P-O-C-C-O-C-C-OH segment; and orbital 319 is relatively dispersed. Therefore, during the $S_0 \rightarrow S_1$ transition at higher excitation energy, the system exhibits a coexistence of Locally Excited (LE) states (orbital 295 to 304), Hybrid Local and Charge-Transfer (HLCT) states (orbital 298 to 307), and Charge-Transfer (CT) states (orbital 299 to 307, orbital 301 to 317/319). Conversely, at the lower excitation energy of 249.98 nm, the oscillator strength is f=0.6147, and the excitation is dominated by the transition from orbital 301 to 307, exhibiting only typical Locally Excited (LE) characteristics.

When two model molecules are used to simulate the aggregated state, at an excitation energy of 252.50 nm, the oscillator strength is f=0.6275. The major contributions to this excitation involve transitions from orbital 599 to 604, orbital 601 to 610, and orbital 602 to 615. Orbital 599 is primarily distributed on the P-C-PhOH segment, while orbital 604 is mainly distributed on the P-C-PhOH segment adjacent to orbital 599. Orbitals 601, 602, and 615 are primarily distributed on the P-C-N-Ph-N segment, and orbital 610 is primarily distributed on the PhOH-C(P=O)-N-Ph-N segment. For the lower excitation energy of 264.01 nm, the oscillator strength is f=0.1431, where the excitation is dominated by the transition from orbital 601 to 608. Orbital 608 is mainly distributed on the PhOH-C(P)-N-Ph-N segment near orbital 601. Both aggregated states exhibit typical Charge-Transfer (CT) characteristics.

Therefore, during the aggregation process of LPPE-αAPB, weak interactions such as hydrogen bonds and van der Waals forces drive the benzene rings and groups like P=O and P-O into close proximity. This close packing not only effectively restricts the motion of intramolecular groups but also significantly enhances the electron exchange and orbital overlap between electron-rich atoms (P, O, N) and the benzene rings. The resulting through-space charge transfer and electron cloud delocalization effects are

continuously strengthened with increasing molecular aggregation. Consequently, aggregation lowers the excitation energy level (HOMO-LUMO gap) of the system, leading to a decrease in the required excitation energy for the molecules, which is macroscopically manifested as a significant red-shift in both excitation and emission wavelengths.

Ionic responsiveness of LPPE-αAPB

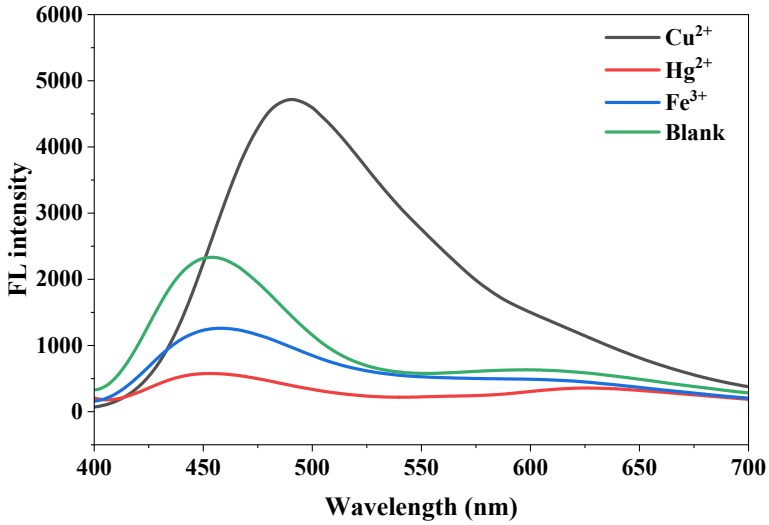

Figure S23. Comparison of fluorescence spectra in the presence of different metal ions in 5 mg/mL LPPE-αAPB aqueous solution

Ionic responsiveness of Schiff 1 and Schiff 2

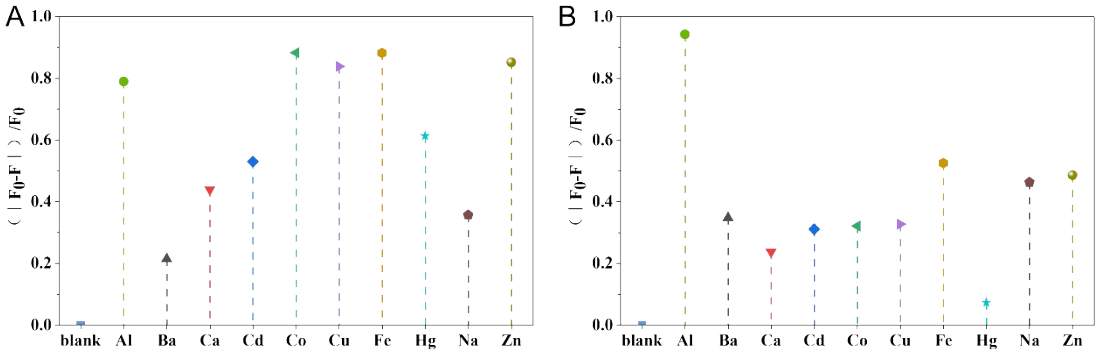

Figure S24. Fluorescence intensity of 5 mg/mL Schiff 1 (A) and Schiff 2 (B) solution in the presence of different metal ions

Analysis: Schiff 1 and Schiff 2, demonstrate that neither exhibits this specific selective response or fluorescence enhancement towards Cu^{2+}. This confirms that the specific Cu^{2+} detection capability is not an intrinsic property of the isolated small molecules but

is enabled by the polymer structure, which provides the necessary coordination environment for the observed response.

CT effect in LPPE-αAPB

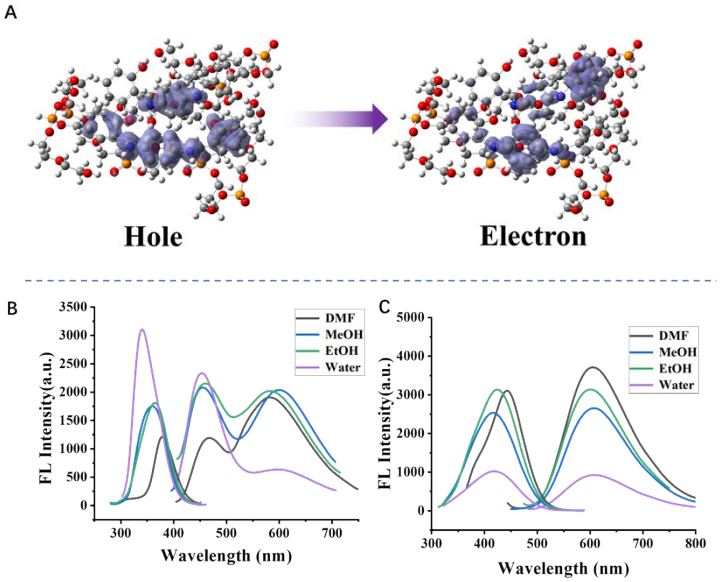

Fig. S25. Electron excitation orbitals of LPPE-αAPB (A); excitation and emission spectra of LPPE-αAPB in different polar solvents (5 mg/mL, Ex=360 nm (B), Ex=430 nm (C)).

Table S4 Summary of excitation and emission wavelengths of 5 mg/mL LPPE-αAPB solution in different solvents

	Excitation Wavelength 1 (nm)	Emission Wavelength 1 (nm)	Excitation Wavelength 2 (nm)	Emission Wavelength 2 (nm)
H_2O	340	453, 610	420	610
MeOH	360	454, 600	416	608
DMF	380	468, 582	443	606
EtOH	367	460, 583	425	600

References

1 N. Ljubijankic, A. Zahirovic, E. Turkusic and E. Kahrovic, Croatica Chemica Acta, 2013, 86, 215-222.
2 S. Guieu, F. Cardona, J. Rocha and A. M. S. Silva, Chemistry – A European Journal, 2018, 24, 17262-17267.